Tanzania Journal of Engineering and Technology 2023, **42**(4):11 - 29
OPEN ACCESS articles distributed under Creative Commons Attribution Licence [CC BY-ND]
Websites: https://ajol.org/tjet; https://tjet.udsm.ac.tz

ISSN 1821-536X (**print**); ISSN 2619-8789 (**electronic**)
https://doi.org/10.52339/tjet.v42i4.849

Regular Research Manuscript

Absorbance Enhancement of a Treated Tanzanian kaolin for Removal of Synthetic Dyes from Water

Laurance Erasto[1,2], Harieth Hellar-Kihampa[1,3†] Quintino Alphonce Mgani[1], and Esther Hellen Jason Lugwisha[1]

[1]Chemistry Department, College of Natural and Applied Sciences, University of Dar es Salaam, P. O. Box 35061, Dar es Salaam, Tanzania

[2]Government Chemist Laboratory Authority, P. O. Box 164, Dar es Salaam, Tanzania

[3]Faculty of Science, Technology and Environmental Studies, The Open University of Tanzania, P. O. Box 23409, Dar es Salaam, Tanzania
[†]Correspondence author email: hhellar@yahoo.co.uk; hariet.hellar@out.ac.tz

[†]ORCID: https://orcid.org/0000-0002-6951-5243

ABSTRACT

The absorbance efficiency of local kaolin clay from Tanzania (Pugu kaolin) has been enhanced to improve its utilization in removal of textile dyes from water. The clay was acid-activated using H_2SO_4, after calcination at 750°C. Characterization by XRF, XRD, ATR-FTIR and Porosimeter showed kaolinite [$Al_2Si_2O_5(OH)_4$], silica (SiO_2) and microcline [$KAlSi_3O_8$] as the main phases. Upon acid treatment, silica increased from 44.18% to 58.81% due to the appearance of tridymite, and alumina decreased from 26.70% to 12.74% due to disappearance of the kaolinite. Surface area increased from 15.36 to 149.61 m^2/g due to removal of acid-soluble impurities. The chemical composition showed decrease of Fe_2O_3 and increase of other major oxides. The impact of acid-activation on contact time, temperature, adsorbent dose, initial pH and absorbate concentration was investigated through batch adsorption technique using basic blue 9 (BB9) and direct red 28 (DR28) dyes. The results at optimal conditions of 3 hours contact time, 27°C temperature, 0.9 g adsorbent dose, initial pH of 11 and initial adsorbate concentration of 90 mg/L, showed that acid modification of the clay increased its capacity to adsorb BB9 from 96.82% to 99.91%, and DR28 from 86.33% to 95.04%. These findings established the influence of modifying the raw clay for its dye removal applications.

ARTICLE INFO

Submitted: **Dec 14, 2022**

Revised: **Nov. 27, 2023**

Accepted: **Dec. 15, 2023**

Published: **Feb., 2024**

Keywords: *batch adsorption technique; clay modification; low-cost adsorbent; kaolin characterization*

INTRODUCTION

The utilization of kaolin clays as potential adsorbent materials in various environmental applications have been widely researched in numerous countries and areas e.g., the Botswana Lobatse clay (Sejie and Nadiye-Tabbiruka, 2016); the Brazilian kaolin (Caponi *et al*., 2017); the Moroccan Rhassoul and Red clays (Bentahar *et al*., 2019); the Ethiopian clay (Aragaw and Angerasa, 2020); (Mulushewa *et al*., 2021) and the Tanzanian Malangali kaolinite (Malima,

2021). One important application of clay adsorbents is removal of synthetic dyes from contaminated waters (Mustapha et al., 2019; Chandan *et al*., 2021). Pollution of surface waters by synthetic dyes is one of the emerging issues of environmental concern. This is particularly due to the fact that there currently exist thousands of commercially available dyes with a wide range of uses in everyday human life. These include fabric colouring in textile industries, production of inks and artistic colours, in food production e.g., soft drinks, sauces and jellies, and in cosmetic industries, e.g., hair dyes. This may cause significant amounts of dye residues to find their ways to water sources during the course of their production and applications. Dye-containing effluents have potential to cause adverse effects if not properly treated, including toxicity to human and aquatic biota, depletion of dissolved oxygen and reduction of amount of light (Berradi *et al*., 2019). Concentration of some dyes at levels exceeding 1 mg/L in water may be visible to the naked eye enough to rise public concerns (Rahman et al., 2015). On the other hand, dyes are inherently designed to be stable to light, heat and oxidizing agents (Avila *et al*., 2021), making their removal from water more complicated. When utilizing clays for dye-removal purposes, efficiency of their absorbance properties is therefore important for realizing the desired outcome. Of recent, modifications of clays to enhance their adsorption efficiency has received continuous attention Nwuzor *et al*., 2018; Gil *et al*., 2021). Some reported kaolin clay modifications methods include alkaline treatment (Zaini *et al*., 2021); surfactant modification (Mudzielwana et al., 2019); hybridization (He *et al*., 2019; Jawad and Abdulhameed, 2020); acid activation (Gao *et al*., 2016) and thermal treatment David *et al*., (2020). The essence of these modifications is to alter the vital clay properties that play important roles in their adsorption properties, such as surface area, ion exchange capacity and chemical and mechanical stability (Li *et al*., 2016).

Tanzania is endowed with probably one of the largest kaolin deposits in the world at Pugu, in Kisarawe District, Coast Region, south west of Dar es Salaam city (UNEP, 2021). The Pugu kaolin clay has been widely investigated pertaining to its applicability in various ways (e.g., Akwilapo and Wiik, 2004; Kimambo *et al*., 2014; Lugwisha and Siafu, 2014). However, its application as an adsorbent in the removal of dyes from polluted water has not been investigated. In this study, the raw Pugu kaolin clay (RPK) is first characterized to establish its chemical and mineralogical compositions, and its performance efficiency in dye removal is tested using basic blue 9 (BB9) and direct red 28 (DR28) dyes as representative adsorbates. The raw clay is then modified through acid activation to obtain acid-activated Pugu kaolin clay (AAPK) with perceived improved quality. The effects of acid activation are investigated, focusing on changes in the mineralogical and chemical compositions, as well as the percentage enhancement of the adsorption efficiency. A series of batch adsorption experiments are conducted using the same two sample dyes to establish the optimum operating parameters for the dyes' removal.

METHODS AND MATERIALS

Chemicals, Reagents and Equipment

All the chemicals used in this study were of analytical grade obtained from certified chemical suppliers. The chemicals included sodium hydroxide (NaOH) of assay 99% obtained from Blulux Laboratories (P) Ltd; hydrochloric acid (HCl) of assay 37% and hydrogen peroxide (H_2O_2) of assay 30% obtained from Scharlau Chemie SA, Spain; sulfuric acid (H_2SO_4) of assay 98% obtained from Fisher Scientific, UK; barium chloride ($BaCl_2$) of assay 98% obtained from J.T. Baker Chemical Company, U.S.A; trihydrated basic blue

dye (BB9) ($C_{16}H_{18}ClN_3S.3H_2O$) of assay 85% obtained from UNI-CHEMI; direct red dye (DR28) ($C_{32}H_{12}N_2Na_2O_6S_2$) of assay 95% obtained from Loba Chemie PVT Ltd and distilled water prepared at the Chemistry Department, University of Dar es Salaam. The instruments used in this study includes alpha ATR-FTIR spectrometer (model: Bruker Optic GmbH 2011, U.S.A), X-ray powder diffractometer (model: BTX 231, Inxitu inc., U.S.A), Nova 1200e Porosimeter (surface area, pore volume and pore diameter analyzer, model: N12-28E, Quantachrome Corporation, Japan) and UV-Vis spectrophotometer (Analytikjena SPECORD 210 PLUS – 223F1376), obtained at the Department of Geosciences, School of Mines and Geosciences, University of Dar es Salaam and X-Ray Fluorescence spectrometer (model: S8 Tiger-SN. 206548, Bruker AXS company, Germany) obtained at the African Minerals and Geosciences Centre, Kunduchi, Dar es Salaam.

Preparation of the raw clay

The clay sample used in this study was obtained from the Pugu clay deposit in Kisarawe District, Coast Region, Tanzania, located at latitude and longitude 6° 52' 29" South and 39° 2' 48" East, respectively. The raw kaolin clay lumps were air dried, crushed, and grinded with mortar and pestle, then sieved through a 300 µm sieve. The resulting fine powdery kaolin was then subjected to the quartering technique to obtain representative sample. The resulting sample was mixed with distilled water and stirred for 4 hours, followed by addition of small amount of hydrogen peroxide (H_2O_2). The mixture was left to settle overnight to allow dissolution of impurities, followed by decantation and vacuum filtration. Thereafter, water was re-added to the kaolin residue and allowed to settle again for 3 hours, which was followed by decantation and filtration to remove more impurities and hydrogen peroxide. This process was repeated four times from which the final obtained kaolin residue was dried in a Genlab oven at 100 ^oC for 12 hours to obtain the RPK, which was stored in an airtight plastic container for later instrumental characterization, preparation of the acid activated clay and running of adsorption studies.

Acid activation treatment of the raw clay

The RPK sample was first calcined at a temperature of 750 ^oC in a muffle furnace for 7 hours, then cooled to room temperature in a desiccator, forming calcined Pugu kaolin (CPK) clay. The obtained CPK was further chemically beneficiated by acid leaching. In the process, five CPK samples, each weighing 50 g were acid leached with 500 mL of 0.1, 0.2, 0.4, 0.8 and 1.2 M sulfuric acid (H_2SO_4) solution, respectively. The process was carried out at 100 ^oC under reflux condition with constant stirring for 3 hours. The resulting suspension was washed through addition of distilled water, followed by vacuum filtration to remove excess sulfuric acid. The filtrate obtained was treated with pre-prepared barium ion (Ba^{2+}) solution to test for the presence of sulfate ion (SO_4^{2-}), whereby barium sulfate ($BaSO_4$) precipitates were formed. The washing process was repeated several times to the point that filtered filtrate did not form precipitates of $BaSO_4$ with barium (Ba^{2+}) solution. This point signified neutral point by which the obtained residue was free of sulfuric acid used during leaching process. The resulting residues were then dried in an oven at 100 ^oC for 12 hours, cooled to room temperature for 3 hours in a desiccator, grinded and re-sieved through 300 µm sieve to obtain the AAPK samples. The adsorbent samples were kept in separate airtight plastic containers for further use in the adsorption studies and determination of the optimal activation concentration of sulfuric acid that would give the AAPK adsorbent the maximum adsorption efficiency.

Preparation of the adsorbates

The standard stock BB9 solution of 1 g/L concentration was prepared by dissolving 0.69 g BB9 powder in distilled water to make 0.5 L of a deep blue solution. The solid powder dye was first dissolved in small amount of distilled water, followed by addition of more water to the mark of the 500 mL flat bottomed volumetric flask, then thoroughly mixed. The standard stock DR28 solution of 1 *g/L* concentration was similarly prepared by dissolving 0.53 g of DR28 powder in 0.5 L of distilled water to form a deep red solution. The two resulting adsorbates solutions were then stored away from light in the plastic bottles for preparation of the BB9 and DR28 adsorbate working solutions that were used in the adsorption studies. These were prepared in the concentration range of 0.1 – 100 mg/L by diluting respective BB9 and DR28 stock solutions based on the dilution law equation:

$$C_i V_i = C_d V_d \quad (1)$$

whereby a given amount of distilled water was added to an initial volume V_i with concentration C_i of the stock solution to make new volume V_d of dilute working solution with desired concentration C_d.

Characterization of the adsorbents

Instrumental characterizations were performed in order to identify functional groups, mineralogical compositions, chemical composition and porosity of the raw as well as the acid activated clay samples. Determination of the available functional groups was performed by ATR-FTIR spectrometer connected to a computer for data manipulation. Small amounts of fine powder samples were pressed against a prism with high refractive index, from which the internally reflected infra-red radiations within the prism gave rise to the respective IR spectra in the range of 400 – 4000 cm^{-1} wavenumbers. The mineralogical compositions were determined by X-Ray powder diffractometer (model: BTX 231) connected to a computer with installed XPowder interface software. About 20 mg of homogeneous fine powder of each of the two clay samples previously prepared, were placed into the sample cell. The samples were then bombarded with generated X-rays by the instrument under operating conditions of temperature of -45 ^oC, voltage of 30.03 kV, and current of 0.30 mA; from which respective XRD patterns for RPK and AAPK were recorded. The d-spacing values for different identified mineral phases for each sample were determined within the position range between 5-55^o 2θ. The elemental compositions, defined by the major oxides of the RPK and the AAK, were determined by S8 Tiger XRF spectrometer with power of 5.2 kVA. About 10 g of fine powder of each sample were mixed with few drops of boric acid, a binding agent, then compressed into circular pellets of 34 mm diameter. The sample pellets were separately introduced into the sample tray of the instrument for analysis of both quantitative and qualitative elemental composition of the samples.

Three physical parameters of surface area, pore volume and pore diameter of the RPK and AAPK samples were analyzed by a Nova 1200e Porosimeter using a nitrogen adsorption-desorption technique at 77.35 K and relative pressure in the range of 0.05 and 0.35. The porosimeter was connected to a computer with NovaWin software installed in it for measurement of surface area, pore volume and pore diameter. About 0.1 g of each RPK and AAPK fine powdery samples were first degassed at 160 ^oC to remove previously physiosorbed contaminants. Then each sample was allowed to interact with liquid nitrogen for adsorption-desorption analysis, from which respective surface area, pore volume and diameter of the samples were obtained.

Batch adsorption experiments

Pre-adsorption Studies

Adsorption studies were preceded by the determination of optimal wavelengths for BB9 and DR28, preparation of calibration curves for respective adsorbates as well as determination of the pH at the Zero Point of Charge (pH_{ZPC}). Maximal absorbances for BB9 and DR28 adsorbates were measured by Analytikjena SPECORD 210 PLUS UV-Vis spectrophotometer. About 3 mL of standard solutions (2.50, 3.00 and 3.50 mg/L of BB9; and 11.50, 15.50 and 18.00 mg/L of DR28) were placed in the cuvette, and then introduced into the instrument for determination of maximum absorbances corresponding to the respective optimal wavelengths for BB9 and DR28. The optimal wavelengths were determined through spectral scan mode within the visible region (350 – 800 nm). These optimal wavelengths were then used in the measurements of the maximum absorbances in the determination of the BB9 and DR28 calibration curves as well as various supernatants obtained in the course of adsorption studies. Several standard solutions of BB9 in the range of 0.1 - 6.0 mg/L at pH of 6.81 and temperature of 27 $^{\circ}$C were prepared, followed by measurements of respective maximum absorbance by UV-Vis spectrophotometer at the predetermined optimal wavelength of 665 nm. In the same way, standard solutions of DR28 in the range of 0.8 - 30 mg/L were prepared, followed by measurements of respective maximum absorbances at the predetermined respective optimal wavelength of 500 nm. In each case, a linear plot of absorbance against concentration were obtained based on the Beer-Lambert's law equation:

$$A = \varepsilon l c \quad (2)$$

where: A = absorbance; l = path length (cm); c = concentration of solution (mol/L) and ε = Molar absorptivity (L mol^{-1} cm^{-1}). The plots were used to determine respective free or equilibrium concentration of each adsorbate dye available in the adsorbent-adsorbate system after given contact time. To determine the pH at the Zero Point of Charge (pH_{ZPC}), ten samples of RPK of 0.5 g each and particle size of 300 µm, were mixed with 0.05 L of distilled water of known initial pH in the range of 2 - 11. Adjustment of pH was attained by addition of few drops of either dilute HCl or NaOH. The systems (water-RPK mixture) were shaken for 12 h at 27 ^{o}C to attain final equilibrium pH. The initial and final pH of each system was measured by digital pH meter. Thereafter determination of the pH_{ZPC} was made from the plot of final pH against initial pH.

Adsorption Studies

In this experiment, the effects of temperature, adsorbent dose, initial pH of adsorbate solution, contact time and initial adsorbate concentration on adsorption efficiency of RPK and AAPK adsorbents were investigated. The experiments were preceded by the determination of the AAPK adsorbent corresponding to the optimal activation concentration of sulfuric acid, which exhibited maximum adsorption efficiency for both BB9 and DR28 adsorbates. In determining of the optimal activation concentration of sulfuric acid, a solution of 0.05 L with 30 mg/L of BB9 adsorbate was added to six adsorbent samples, each weighing 0.5 g and particle size of 300 µm. Out of these adsorbents, five samples were of AAPK leached with 0.1, 0.2, 0.4, 0.8 and 1.2 M H_2SO_4 and one was of RPK as a reference sample. The pH of each system was then adjusted to 6.80 by addition of few drops of either HCl or NaOH dilute solution. In a similar manner, DR28-adsorbent systems were prepared. This pair of systems were then shaken at 26.5 ^{o}C for 3 hours. Thereafter, each system was centrifuged for 15 min at 4000 rpm to obtain respective supernatants for determination of the free concentration of BB9 and DR28, and adsorption efficiency of each adsorbent. These data were used in determination of AAPK adsorbent corresponding to the optimal activation concentration of sulfuric acid that gave maximum adsorption efficiency. The

respective AAPK with maximum adsorption efficiency was used for further adsorption studies. To determine the free concentration for each adsorbate, about 3 mL of each supernatant dye solution obtained from adsorbate-adsorbent systems were placed in a cuvette for the measurement of absorbances by UV-Vis spectrophotometer at the pre-determined optimal wavelengths of λ = 665 nm and 500 nm for BB9 and DR28 solutions, respectively. These absorbances were then converted to corresponding equilibrium concentration from predetermined BB9 and DR28 calibration curves.

Determination of the adsorption phenomenon

Adsorption isotherms were used to describe adsorption equilibrium attained between adsorbent and adsorbate. Such equilibrium is essential in understanding the adsorption mechanism as well as the nature of adsorbent, adsorbate and respective intermolecular forces (Sharma 2015). They were also used to determine the thermodynamic data that play the central role in determining the spontaneity, viability and favorability of the adsorption phenomenon. In this study, the Langmuir and Freundlich isotherms were used to examine the nature of the adsorption process between the BB9 and DR28 adsorbates and the RPK and AAPK adsorbents.

The Langmuir adsorption isotherm (LAI) model characterizes ideal monolayer homogeneous adsorption, in which all adsorbent's adsorptive sites have equal energy and equally available. In addition, it defines adsorption with neither interaction between adsorbed molecule nor transmigration of adsorbate molecules into the adsorbent surface. The linear form of the isotherm can be explained by the equation (Liu *et al*., 2019):

$$\frac{c_e}{q_e} = \frac{1}{bq_m} + \frac{c_e}{q_m} \quad (3)$$

where: b = Langmuir constant (L mg $^{-1}$) which is related to adsorption energy, q_e = quantity of adsorbate adsorbed per unit adsorbent mass (mg/g), c_e = free or equilibrium concentration of adsorbate (mg/L), q_m = maximum adsorbent adsorption capacity (mg/g).

The Freundlich adsorption isotherm (FAI) describes non-ideal adsorption onto heterogeneous adsorbent surface, with assumption that adsorbate concentration is directly related to the amount of adsorbate adsorbed. It is described by the equation (Singh, 2016):

$$lnq_e = lnK_f + \left(1/n\right) lnc_e \quad (4)$$

where: q_e = amount of adsorbate adsorbed per unit mass of adsorbent at equilibrium (mg/g); c_e = free or equilibrium concentration of the adsorbate dye (mg/L); $1/n$ = measure of adsorption intensity and K_f = Freundlich constant that define measure of adsorption capacity.

RESULTS AND DISCUSSION

Characterization of the raw and acid-activated clays

Functional Groups: The ATR-FTIR absorption bands [Wavenumber (cm^{-1})] for RPK and AAPK adsorbents are shown in Figure 1(a) and (b). It shows that the RPK exhibited absorption peaks at 788.67 (stretching vibration) and 752.92 cm^{-1} (bending vibration) corresponding to pure kaolinite; while sharp peaks at 3687.28 and 3619.17 cm^{-1} (stretching vibrations) imply the presence of crystalline kaolinite in the RPK sample. In addition, the peaks at 688.06, 533.44 and 462.37 cm^{-1} (stretching vibrations) also suggested the availability of kaolinite in the sample (Nayak and Singh, 2007).

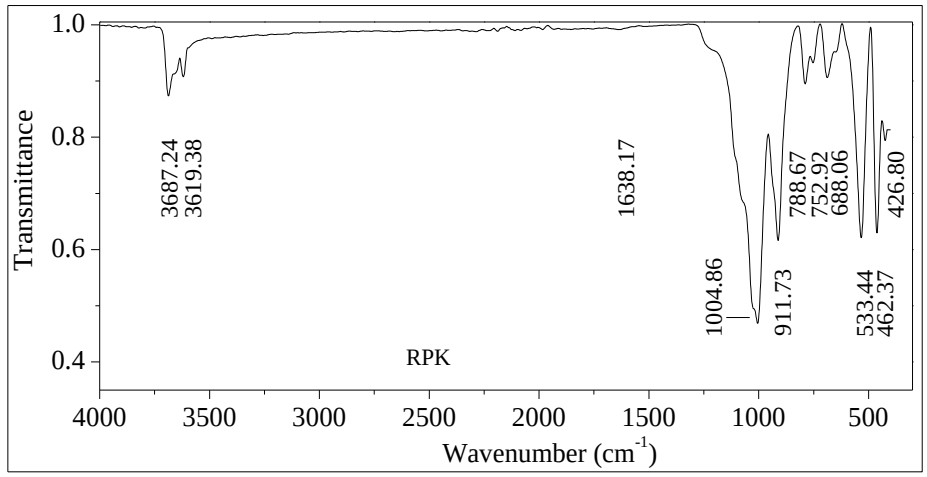

(a)

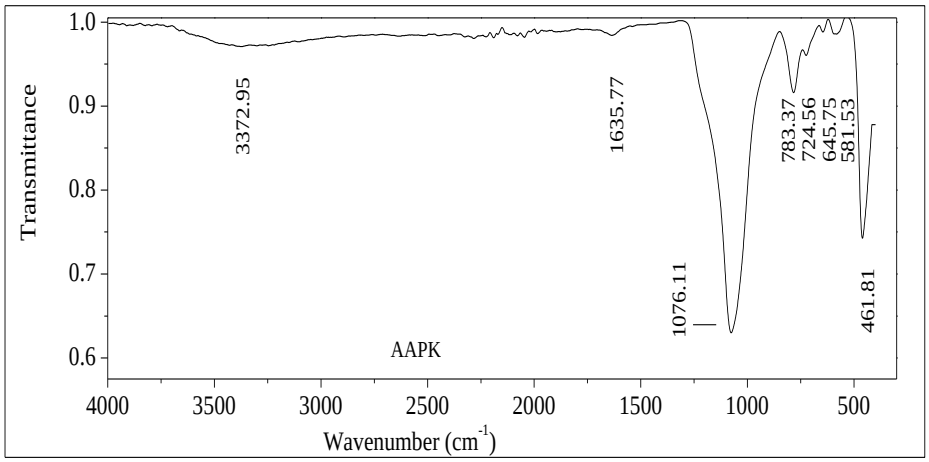

(b)

Figure 1: ATR-FTIR Spectra of RPK (a) and AAPK (b) showing the different absorption bands before and after treatment

The AAPK adsorbent exhibited an ATR-FTIR spectrum which is different from that of RPK, where the peak intensities had been reduced while some bands had shifted. Figures 1 also show that upon acid activation of the raw clay, the 3687.24 and 3619.38cm^{-1} (stretching vibrations) bands were transformed into a very broad peak and shifted to 3372.92 (stretching vibration); while the peak at 752.92 cm^{-1} shifted to 724.56 cm^{-1} (bending vibration), and that at 688.06 shifted to 645.75 cm^{-1} (stretching vibrations). These changes suggested structural changes of the RPK upon calcination followed by acid leaching in the formation of AAPK. Structural changes were further described by the disappearance of the 426.80 (bending), 911.73 and 1004.86 cm^{-1} (stretching vibrations) peaks as well as the appearance of the new peak at 1076.11 cm^{-1}(stretching vibration). The new peak proposed the presence of amorphous silica (Boukhemkhem and Rida, 2017). The shift of the sharp peak at 533.44 cm^{-1} to broad peak at 581.53 cm^{-1} (stretching vibrations) with much reduced peak intensity also further support structural changes of the RPK upon acid activation. The observations made reflected the loss of the crystalline nature of kaolinite in kaolin. Such observation is in good agreement with findings from other researchers (e.g., Gao *et al*. 2016; Boukhemkhem and Rida, 2017).

Figure 2 compares the ATR-FTIR spectra before and after adsorption. It indicates that almost all absorption bands remained the

same but with reduced intensities after adsorption, implying that the physisorption between RPK and AAPK adsorbents and adsorbates (BB9 and DR28) predominated over chemisorption.

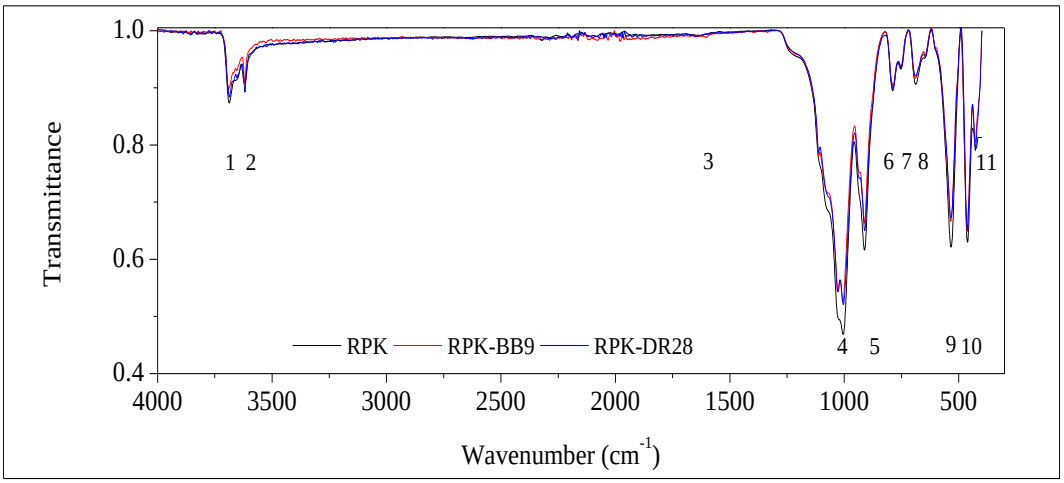

(a)

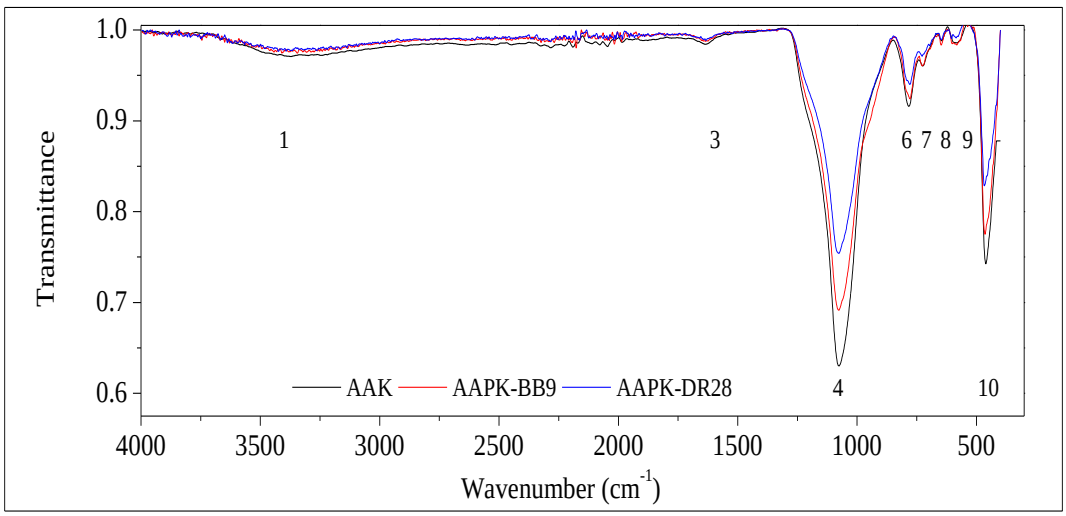

(b)

Figure 2: ATR-FTIR Spectra of RPK (a) and AAPK (b) showing the different adsorption bands before and after adsorption of the two dyes.

The decreased peak intensities of RPK and AAPK suggested that exposure of the respective adsorbent functional groups as a result of BB9 and DR28 adsorption were reduced. Furthermore, in all two cases, peaks corresponding to DR28 adsorption are much reduced than the peaks for BB9 adsorption. In other way, BB9 adsorption resulted into a more ordered kaolinite than DR28, which is fairly in good agreement with observed entropy values obtained in this study. The observation is closely related to the ones reported by other researchers (e.g., Monash *et al*., 2011).

Mineralogical Composition

Figure 3 compares the XRD patterns of the raw (RPK) and activated (AAPK) clays

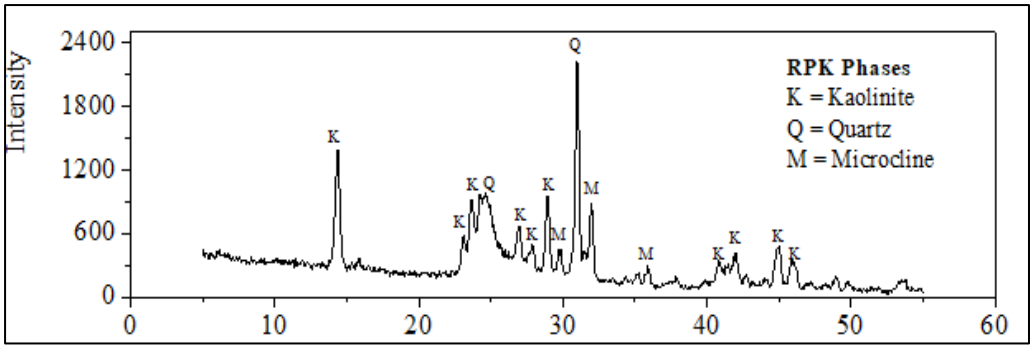

(a)

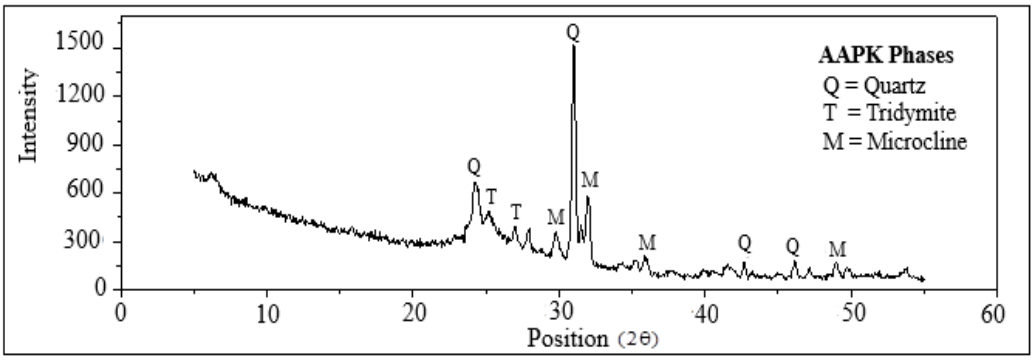

(b)

Figure 3: XRD patterns for RPK (a) and AAPK (b) showing the different mineralogical phases before and after treatment

The XRD pattern for the RPK in Figure 3(a) identifies three phases i.e., kaolinite [$Al_2Si_2O_5(OH)_4$], quartz (SiO_2) and potassium feldspar or microcline [$KAlSi_3O_8$] as impurities in the kaolin sample. Microcline is a raw material that can decompose into kaolinite under proper condition (Omang *et al*., 2019). Among the important peaks obtained include reflections corresponding to the d values of 7.16, 4.35, 3.58 and 3.84 Å at position around 2θ =14.40º, 23.5º, 29º and 26.90º, respectively, for kaolinite. This is in good agreement with the previous reported findings (Lugwisha and Siafu, 2014; Lugwisha and Lunyungu, 2016), hence it can be inferred that the raw kaolin used in this study contained crystalline kaolinite with coarser grains. The microcline phase identification was based on the reflection giving several peaks, including major peaks defined by d values of 3.25 and 3.48 Å approximately to 2θ = 32º and 30º, respectively. Identification of quartz, a polymorph of silica phase in RPK sample was based on the presence of prominent reflection peak of d value corresponding to 3.35 and 4.2 Å at position approximately to 2θ = 31º and 24.5º, respectively.

The XRD pattern of AAPK (Figure 3b) indicates the presence of phases of microcline and two polymorphs of silica (quartz and tridymite); and the disappearance of the kaolinite phase. Tridymite was identified with reflection peaks at d values of 4.10, 3.82 Å approximately to position of 25º and 27º 2θ, respectively. The presence of tridymite silica might be the result of calcination reaction of the kaolin clay at 750 ºC which accounts for increased silica content in the AAPK sample as it has been observed from XRF analysis in this study. Microcline and quartz maintained their prominent d values of 3.25 and 3.48 Å approximately to 32º and 30º 2θ, respectively, for microcline. For quartz, the d values were 3.35 and 4.20 Å approximately to 31º and 24.5º 2θ. Such observation implies that quartz and

microcline were not affected by acid activation, similar to what was observed by other researchers (e.g., Luo *et al*. 2016). Calcination of kaolin at 750 ^{o}C probably accounts for the primary disappearance of kaolinite peaks resulting into the formation of a powderier amorphous metakaolin as a result of dihydroxylation (Luo *et al*., 2016). Acid leaching of the calcined kaolin accounts for further structural changes of raw kaolin due to dissolution of structural Al^{3+} ions, resulting into residue with increased silica content. Such finding is in good agreement with the finding reported by other researchers (Boukhemkhem and Rida, 2017; Luo *et al*., 2017). The finding also correlates well with the observed decreased percent composition of Al_2O_3 and the increased silica (SiO_2) content from XRF analysis in this study.

Chemical composition

Chemical compositions of the RPK and AAPK in terms of nine major oxides are summarized in Table 1. The silica (SiO_2) and alumina (Al_2O_3) contents of the raw clay are in good agreement with those reported in another study of the Pugu kaolin (Akwilapo and Wiik, 2004). The results show that six of the oxides i.e., SiO_2, CaO, K_2O, Na_2O, MnO and P_2O_5 increased after acid activation by various degrees, while three of the oxides decreased. The changes in percentage compositions of the AAPK compared to the RPK imply occurrences of structural and surface modification resulting into more exposure of the adsorptive sites. Hence increasing its absorbance efficiency, as was also observed by Gao *et al*. (2016). The increase in the silica content from 44.18% to 58,81% after acid activation corresponds to the appearance of the tridymite phase; while the decrease in the alumina content from 26.70% to 12.74% corresponds to the disappearance of the kaolinite phase, as supported by the XRD results. Furthermore, the alumina might have decreased due to the dissolution of dialuminium silicate during acid leaching as per the chemical equation $Al_2Si_2O_{7(s)} + 3H_2SO_{4(aq)} \rightarrow Al_2(SO_4)_{3(s)} + 2SiO_2(s) + 3H_2O_{(l)}$.

Table 1: Chemical compositions of the raw (RPK) and acid-activated (AAPK) clays

Constituent	RPK Composition (%)	AAPK Composition (%)
SiO_2	44.18	58.81
Al_2O_3	26.70	12.74
Fe_2O_3	1.78	0.82
CaO	13.01	14.53
MgO	0.54	0.12
K_2O	1.73	1.87
Na_2O	0.04	0.07
MnO	0.02	0.05
P_2O_5	0.06	0.08
LOI	11.9	10.88

Physical parameters

The results from the porosimeter characterization indicated specific surface areas of 15.36 m^2/g and 149.61 m^2/g; pore volumes of 0.033 cm^3/g and 0.026 cm^3/g; and pore diameters of 3.049 nm and 28.200 nm for the raw and acid activated clays,

respectively. Comparison of the three parameters for the raw and acid activated clays showed that specific surface area of the raw clay was relatively low in a way that may render the adsorption efficiency of the raw clay to be insufficient, supporting the necessity of its modification. The almost ten-fold increase of the surface area upon acid activation was significantly high to enable physical modification of the clay. Previous studies had indicated that calcination of raw kaolin at temperatures above 150 ^{o}C has a potential to remove impurities including adsorbed water, which results into increased surface area and exposure of the adsorptive sites (Avila *et al*., 2021). Calcination of kaolin at a temperature of 750 ^{o}C employed in this study therefore removed the unwanted impurities and also transformed kaolin into porous amorphous metakaolin characterized by increased surface area. The formation of amorphous metakaolin was also supported by the XRD pattern in Figure 3, which indicated the disappearance of crystalline kaolinite in the AAPK phases. Acid leaching of the calcined kaolin further removed any remained impurities that are acid soluble, resulting into further increased surface area. With respect to the pore volume, the aggregation of fine particles probably accounts for the decreased pore volume of the AAPK relative to the RPK. Similar observation was also reported by Monash *et al*. (2011) and Boukhemkhem and Rida (2017). The pore diameter of the AAPK increased almost nine-folds, which also indicates significant modification to its properties.

Optimal conditions for adsorption efficiency

Concentration of sulfuric acid

Figure 4 compares adsorption efficiencies of the modified clay after leaching with varied concentrations of H_2SO_4, using the two sample dyes, i.e., BB9 and DR28. It shows that the concentration of 0.2 M H_2SO_4 gave the highest adsorption of 96.96% and 93.55% for BB9 and DR28, respectively compared to that of the raw clay, which were 75.02% for BB9 and 34.16% for DR28. Activation with 0.2 M sulfuric acid gave the maximum increment in surface area to 149.61 m^2/g. These results indicate that 0.2 M can be regarded as the optimal activation concentration of H_2SO_4.

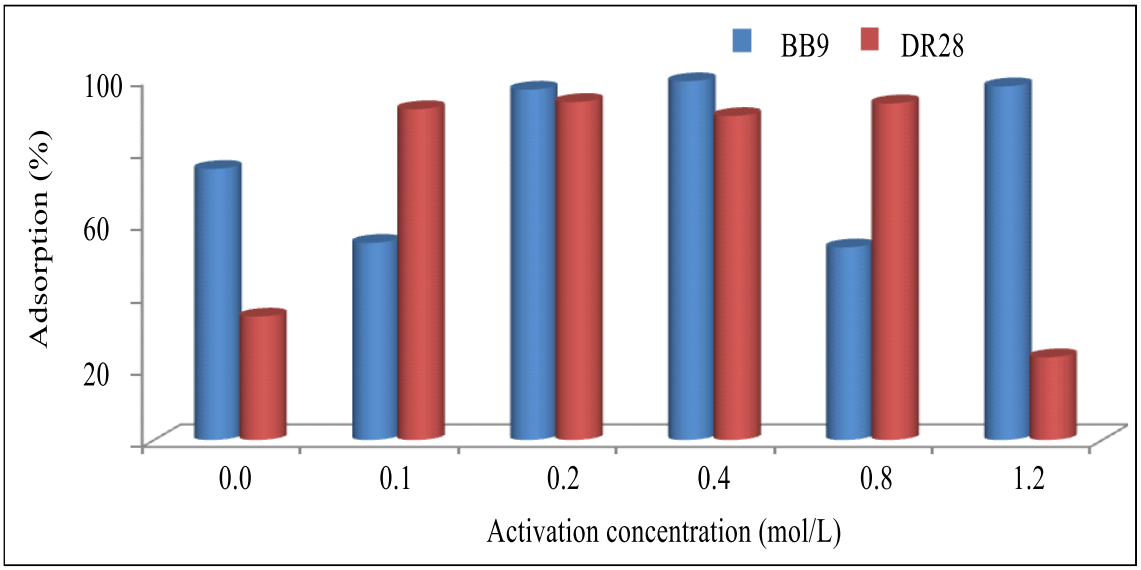

Figure 4: Adsorption efficiency of the modified clay for the two dyes at different H_2SO_4 activation concentrations.

Operational Parameters

Temperature

Table 2 summarizes the results of the effect of temperature on adsorption efficiency of adsorbents. The adsorption efficiency and quantity adsorbed per unit mass of adsorbent for BB9 and DR28 decreased as the temperature was raised from 27 to 90 °C in the order of RPK < AAPK.

Table 2: Effect of temperature on adsorption of BB9 and DR28

Adsorbent	*Temp* (°C)	DR28			BB9		
		c_e (mg/L)	A_e (%)	q_e (mg/g)	c_e (mg/L)	A_e (%)	q_e (mg/g)
RPK	27	14.488	51.71	1.551	5.566	81.45	2.443
	43	15.068	49.77	1.493	7.963	73.46	2.204
	56	16.347	45.51	1.365	8.241	72.53	2.176
	76	17.883	40.39	1.212	9.995	66.68	2.000
	90	18.412	38.63	1.159	11.527	61.58	1.847
AAPK	27	11.264	62.45	1.874	1.014	96.62	2.899
	43	11.369	62.10	1.863	1.400	95.33	2.860
	56	12.492	58.36	1.751	2.128	92.91	2.787
	76	13.850	53.83	1.615	4.070	86.43	2.593
	90	16.575	44.75	1.343	5.630	81.23	2.437

The data in Table 2 show that BB9 was adsorbed more with adsorption efficiency from 81.45 to 61.58% for RPK and 96.62% to 81.23% for AAPK; while for DR28, the adsorption efficiency decreased from 51.71% to 38.63% for RPK and 62.45% to 44.75% for AAPK. The observed trend implies that the adsorption processes were more favorable at low temperature and exothermic in nature. The exothermic nature of the adsorption process is supported by the negative values of the enthalpy change. The trend agrees with thermochemistry concept that is exothermic process usually become more favorable as temperature decreases and the vice versa for endothermic reaction. The variation of in adsorption efficiency was proportion to the surface area of the adsorbents. These results are comparable to the one previously reported in the literature (e.g., Sejie and Nadiye-Tabbiruka, 2016).

Adsorbent dose

Table 3 summarizes the effect of adsorbent dose on adsorption of the two dyes. It shows that the adsorption efficiency of adsorbents (A_e) increased and the quantity of adsorbate adsorbed per unit mass of adsorbent (q_e) decreased as the adsorbent dose increased. The data in Table 3 show the adsorption efficiency of BB9 increased from 40.82% to 96.82% for RPK and from 69.54% to 99.74% for AAPK; whereas that of DR28 increased from 25.62% to 46.11% for RPK and 31.82% to 82.08% for AAPK.

Table 3: The effect of adsorbent dose on BB9 and DR28 Adsorption

Adsorbent	**Dose (g)**	**BB9**			**DR28**		
		c_e (mg/L)	A_e (%)	q_e (mg/g)	c_e (mg/L)	A_e (%)	q_e (mg/g)
RPK	0.1	17.755	40.82	6.123	22.315	25.62	3.843
	0.3	10.590	64.70	3.235	20.346	32.18	1.609
	0.5	4.801	84.00	2.520	18.711	37.63	1.129

	0.7	2.209	92.64	1.985	18.194	39.35	0.843
	0.9	0.955	96.82	1.614	16.167	46.11	0.768
AAPK	0.1	9.137	69.54	10.431	20.455	31.82	4.772
	0.3	1.846	93.85	4.692	17.003	43.32	2.166
	0.5	0.971	96.76	2.903	12.266	59.11	1.773
	0.7	0.338	98.87	2.119	10.156	66.15	1.417
	0.9	0.077	99.74	1.662	5.376	82.08	1.368

The increased adsorbent dose account for increased adsorptive sites and surface area hence increased adsorption efficiency as well. In general, kaolin clay possesses negative structural charge hence strong affinity to the cationic adsorbates compared to an anionic adsorbate. The second reason might be the molecular size of the adsorbates. BB9 has small molecular size hence exert weak intra-repulsion force per unit adsorptive sites while DR28 is likely to exert strong intra-repulsion forces per unit adsorptive site. Another possible explanation on the observed trends is that adsorption capacity is determined by assuming every adsorbent molecule is saturated with adsorbate molecules at equilibrium. For low adsorbent dose this assumption was approximately obeyed while for higher dose adsorbent molecules were not saturated with adsorbate molecules. As a result, adsorption capacity for higher adsorbent dose become smaller compared to the lower adsorbent dose. Such variations were also observed by Nandi *et al*. (2009).

Initial pH

Figure 5 summarizes results of the effect of initial pH on adsorption efficiency of the two dyes. As the initial pH increased from 3, 5, 7, 9 to 11, the adsorption efficiency of BB9 increased from 68.71% to 94.73% for RPK and 94.13% to 98.85% for the AAPK at a pH value of 11, whereas for the DR28 it increased to the optimal adsorption of 86.33% for RPK and 94.03% for AAPK at pH value of 5, then decreased to the value of 56.86% for RPK, 63.44% and 67.83% for AAPK at pH value of 11.

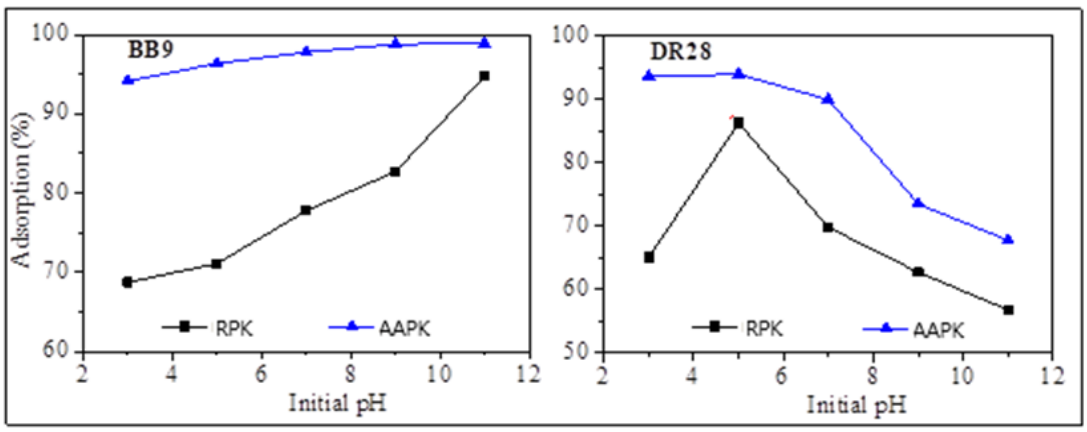

Figure 5: The effect of initial solution pH on adsorption of BB9 and DR28.

The higher BB9 adsorption likely was due to the increased electrostatic interaction between cationic BB9 and adsorbents arising from increased strength of negative charge on respective adsorbents as pH increased. At the pH of 5 which is less than the pH_{ZPC} (6.04) (Nandi *et al*., 2009), the adsorbents developed more surface positive charge accounting for observed optimal adsorption. However, at

much lower pH than 5, probably there are strong competitions for developed positive surface charge resulting into repulsion between the relatively large molecules of DR28 adsorbates. The effect of such repulsion account for observed decreased adsorption efficiency. Furthermore, at pH greater than the pH_{ZPC} adsorbents began to develop negative charge hence account for decreased adsorption as pH increased due to repulsion between negative surface charge and charge of the anionic DR28 adsorbate (Olaremu, 2015).

Contact Time

Table 4 summarizes the results of variation of adsorption efficiency of both BB9 and DR28 with varying contact time from 0, 20, 60, 100 140 to 180 minutes.

Table 4: Effect of the contact time on BB9 and DR28 Adsorption

Adsorbent	Time (min)	BB9			DR28		
		c_e (mg/L)	A_e (%)	q_e (mg/g)	c_e (mg/L)	A_e (%)	q_e(mg/g)
RPK	20	4.922	83.60	2.508	17.473	41.76	1.253
	60	3.221	89.26	2.678	15.565	48.12	1.444
	100	3.072	89.76	2.693	15.507	48.31	1.449
	140	2.599	91.34	2.740	15.059	49.80	1.494
	180	2.566	91.45	2.743	14.983	50.06	1.502
AAPK	20	0.225	99.25	2.977	15.171	49.43	1.483
	60	0.097	99.68	2.990	13.492	55.025	1.651
	100	0.056	99.81	2.994	13.247	55.84	1.675
	140	0.051	99.83	2.995	12.725	57.58	1.727
	180	0.028	99.91	2.997	12.193	59.36	1.781

The data in Table 4 show that the adsorption efficiency of both BB9 and DR28 increased with contact, however, in comparing the two dyes, the BB9 was adsorbed more compared to DR28. This indicates the importance of the dye type as well.The adsorption rate was found to be faster in the first 20 min of contact time, from which adsorption efficiency of BB9 increased to 83.59% and 99.25% for RPK and AAPK, respectively, while for DR28, the observed adsorption efficiencies were 41.76% and 49.43% for RPK and AAPK respectively. Thereafter percent color removal increased slowly to about equilibrium within contact time of 180 min. The maximum adsorptions were found to be 91.45% and 99.91% BB9 for RPK and AAPK respectively; while for DR28 observed optimal adsorption were 50.06% and 59.36% for RPK and AAPK respectively. The higher adsorption rate in the first few minutes of contact time accounts for availability of enough free adsorptive sites as well as surface area of the adsorbents. Later on, number of free adsorptive sites and surface area decreased with increased contact time accounting for the observed slower adsorption rate. The attachment of adsorbate molecules onto the surface of the adsorbent account for decreased surface area as well as adsorptive sites available for further adsorption. Similar observations of the adsorption behavior of kaolin as a function of contact time have also been reported by other researchers (e.g., Lugwisha and Lunyungu, 2016)

Initial Concentration

The variation of the quantity of adsorbate adsorbed (q_e) with increased initial adsorbate concentration from 30, 45, 60, 75 to 90 mg/L showed that the activated clay AAPK achieved the highest adsorption capacity with optimal q_e of 6.429 and 8.634 mg/g

respectively of BB9, and 4.232 and 6.917 mg/g of DR28 at initial concentration of 90 mg/L. Increasing adsorbate concentration accounts for increased adsorbate molecules resulting into increased amount adsorbed per unit mass of adsorbent. On the other hand, the percent of color removal decreased with increased initial adsorbate concentration. The observation can be explained in terms of available surface area relative to the number of adsorbate molecules available. For adsorption system with initial higher concentration; available adsorbent surface area as well as adsorptive sites are not enough to adsorb available large number of adsorbate molecules to great extent compared to the adsorption system with initial lower adsorbate concentration. As a result, adsorption system with initial higher concentration exhibited higher equilibrium concentration than system with initial lower concentration; thus, accounting for observed decreased color removal with increased initial adsorbate concentration. This suggests more contact time and adsorbent dose are required under condition of initial high concentration of adsorbates for effective color removal, similar to what was observed by Sejie and Nadiye-Tabbiruka (2016). In general, both RPK and AAPK adsorbents indicated similar trend of the adsorption efficiency against BB9 and DR28 adsorbates. BB9 was adsorbed more than DR28 for both adsorbents, which is likely due to the fact that kaolin naturally possesses negative charge hence exhibiting strong affinity against cationic adsorbates compared to anionic adsorbates (Kumar *et al*., 2013).

Adsorption Isotherms

The Langmuir and Freundlich adsorption isotherms for the two systems are presented in Figure 6. The Langmuir isotherms are linear with respective correlation coefficient (R^2) values of 0.983 and 0.975 for the RPK-BB9 and the AAPK-BB9 systems respectively, and 0.982 and 0.989 for the RPK-DR28 and the AAPK-DR28 systems respectively.

These R values that are close to unit, together with the obtained values of separation factor S_f that ranged between 0 and 1 ($0 < S_f < 1$) suggest favourable monolayer adsorption as it has been also reported by Boukhemkhem and Rida (2017) and Patabandige *et al*., (2019). However, the smaller value of S_f implies strong interaction between adsorbate and adsorbents hence it likely indicates less reversibility of the adsorption process. Further analysis of the S_f indicated that BB9 bound a bit stronger to the adsorbents than DR28 in the AAPK than the RPK, supporting the fact that BB9 was more adsorbed than DR28 as it has been pointed out earlier.

The Freundlich adsorption isotherms for the two dyes are linear with correlation coefficient values (R^2) of 0.906 and 0.924 for the RPK-DR28 and AAPK-DR28 adsorption systems respectively, while those for the RPK-BB9 and AAPK-BB9 systems corresponding to coefficient values of 0.900 and 0.990, respectively. The R^2 values that are approaching unit, together with the obtained values of adsorption intensity (n) in the range of 2-10 suggest favourable and multilayer adsorption of adsorbates onto heterogeneous adsorbent surface. However, the activated kaolin showed better adsorption than the raw kaolin due to the respective higher values of adsorption intensity. Comparable findings have been reported by Boukhemkhem and Rida (2017). The BBP adsorbent system displayed lower values of Gibb's free energy at various temperature ranges than the DR28 adsorption system, implying that the respective adsorption process was more feasible and spontaneous for the BB9 system. This likely also account for higher adsorption of BB9 than DR28.

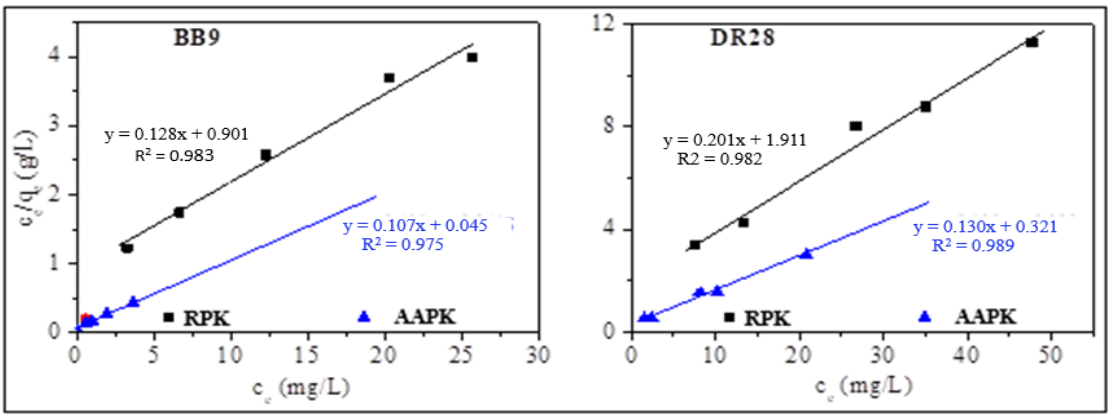

(a)

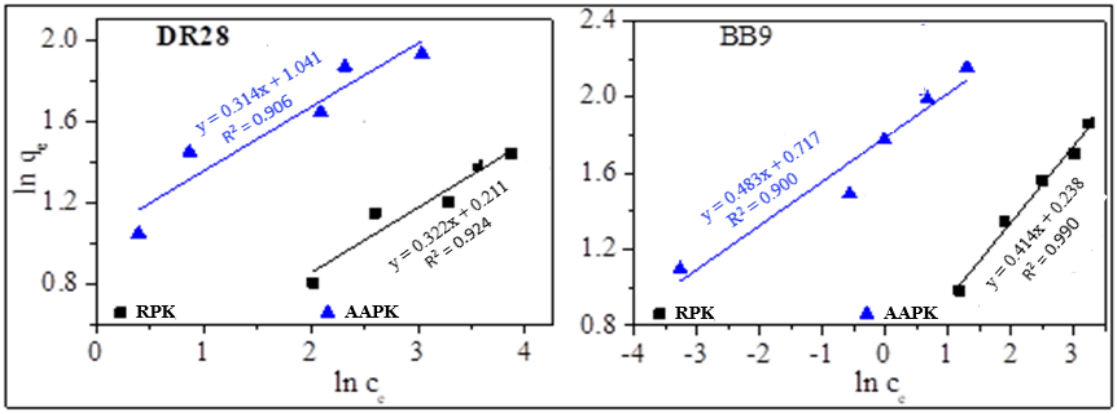

(b)

Figure 6: (a) Langmuir adsorption isotherms (b) Freundlich adsorption isotherms for the two dyes.

CONCLUSION AND RECOMMENDATION

This study explored the outcomes as well as the optimal conditions of treating a local clay from Tanzania (Pugu kaolin clay) for the purpose of enhancing its absorbance efficiency in removing synthetic dyes from water. It employed the adsorption technique in varied conditions, using BB9 and DR28 as representative water-soluble dyes. Characterization by ATR-FTIR, XRD and XRF show that the raw clay exhibited absorption bands that reflect the presence of crystalline kaolinite with physisorbed water [$Al_2Si_2O_5(OH)_4$], silica (SiO_2) and microcline [$KAlSi_3O_8$] phases, whereas upon acid activation, the silica content increased while the alumina content decreased due to loss of the kaolinite phase. The modified kaolin clay which was obtained after calcination at 750 ^oC followed by acid activation using H_2SO_4 at various concentrations, had a more suitable adsorption capacity for the removal of the two dyes compared to the raw clay. The higher adsorption capacity was attributed to increased specific surface area and structural changes that came from removal of some impurities. The H_2SO_4 concentration of 0.2 M was found to provide the optimal activation with adsorption efficiency of 96.96% and 93.55% for BB9 and DR28, respectively.

The study further investigated the effects of various operating parameters that usually affect adsorption efficiency of the adsorbents, including temperature, contact time, initial pH of adsorbate, initial concentration of adsorbate and adsorbent dose on adsorption of the two dyes by the raw and activated adsorbents. It was found that the optimal conditions of 3 hours contact time, 27^oC temperature, 0.9 g adsorbent dose, initial pH of 11 and initial adsorbate concentration of 90

mg/L, gave increased adsorption efficiency from 96.82% to 99.91% for BB9, and from 86.33% to 95.04% for DR28. Although the raw kaolin clay exhibited relatively weaker interactions with the adsorbates than its activated form, still the obtained efficiency was sufficiently reasonable, especially for BB9, in such a way that it can also be used directly without modification. The isotherm and kinetic models for the adsorption conform to the Langmuir and Freundlich models, with high values of correlation coefficients, which suggest that the adsorption process follow the monolayer-multilayer adsorption mode between the adsorbates and the adsorbents. These results provide useful information on the use of Pugu kaolin clay found in Tanzania, as a low-priced, non-hazardous and efficient adsorbent in removal of textile dyes from contaminated water.

Acknowledgements

The authors appreciate the contributions of technical staff at the Department of Geosciences, School of Mines and Geosciences, University of Dar es Salaam and the African Minerals and Geosciences Centre, Kunduchi, Dar es Salaam in carrying out the instrumental analyses for this study.

Authors' Contributions

Laurance Erasto: Conceptualization, methodology, investigation, data curation. Harieth Hellar-Kihampa: Writing of original draft, visualization. Quentin Alphonce Mgani: Conceptualization, methodology, supervision. Esther Hellen Lugwisha: Conceptualization, methodology, supervision, mentorship.

Declarations

The authors declare no conflict of interest.

REFERENCES

Akwilapo L.D. and Wiik K. (2004). Ceramic properties of pugu kaolin clays. Part 2: Effect of phase composition on flexural strength. *Bull. Chem. Soc. Ethiopia*., **18**, 1-10. https://doi.org/10.4314/bcse.v18i1.61631

Aragaw, T.A. and Angerasa, F.T. (2020). Synthesis and characterization of Ethiopian kaolin for the removal of basic yellow (BY 28) dye from aqueous solution as a potential adsorbent. *Heliyon* **6**, e04975. https://doi.org/10.1016/j.heliyon.2020.e04975

Avila, M.C., Lick, I.D., Comelli, N.A. and Ruiz, M.L. (2021). Adsorption of an anionic dye from aqueous solution on a treated clay. *Groundwater Sustain. Dev.*, **15**, 100688, https://doi.org/10.1016/j.gsd.2021.100688

Bentahar, Y., Draoui, K., Hurel, C., Ajouyed, O., Khairoun, S. and Marmier, N. (2019). Physico-chemical characterization and valorization of swelling and non-swelling Moroccan clays in basic dye removal from aqueous solutions. *J African Earth Sci.*, **154**, 80-88. https://doi.org/10.1016/j.jafrearsci.2019.03.017

Berradi, M., Hsissou, R., Khudhair, M., Assouag, M., Cherkaoui, O., El Bachiri, A and El Harfi, A. (2019). Textile finishing dyes and their impact on aquatic environs. *Heliyon* **5**(11), e02711. https://doi.org/10.1016/j.heliyon.2019.e02711

Boukhemkhem, A. and Rida, K. (2017). Improvement adsorption capacity of methylene blue onto modified tamazert kaolin. *Adsorption Sci Technol*., **35**(9-10), 1-21. https://doi.org/10.1177/0263617416684835

Caponi, N., Collazzo, G.C., Jahn, S.L., Dotto, G.L., Mazutti, M.A. and Foletto, E.L. (2017). Use of Brazilian kaolin as a potential low-cost adsorbent for the removal of malachite green from colored effluents. *Mater. Res.*, **20**, 2014-2022. https://doi.org/10.1590/1980-5373-MR-2016-0673

Chandan, M.R., Goyal, S., Rizwan, M., Imran, M. and Shaik, A.H. (2021). Removal of textile dye from synthetic wastewater using microporous polymer nanocomposite. *Bull. Mater. Sci.*, **44**, 272. https://doi.org/10.1007/s12034-021-02559-3

David, M.K., Okoro, U.C., Akpomie, K.G., Okey, C. and Oluwasola, H.O. (2020).

Thermal and hydrothermal alkaline modification of kaolin for the adsorptive removal of lead (II) ions from aqueous solution. *SN Appl. Sci.* **2**, 1134. https://doi.org/10.1007/s42452-020-2621-7

Gao, W., Zhao, S., Wu, H., Deligeer, W., and Asuha, S. (2016). Direct acid activation of kaolinite and its effects on the adsorption of methylene blue. *Appl Clay Sci* **126**, 98-106. https://doi.org/10.10160/j.clay.2016.03.006

Gil, A., Santamaría, L., Korili, S.A., Vicente, M.A., Barbosa, L.V. and de Souza S.D. (2021). A review of organic-inorganic hybrid clay-based adsorbents for contaminants removal: Synthesis, perspectives and applications. *J. Environ. Chem. Engrg*. **9**, 105808. https://doi.org/10.1016/j.jece.2021.105808

He, K., Zeng, G., Chen, A., Huang, Z., Peng, M., Huang, T. and Chen, G. (2019). Graphene hybridized polydopamine-kaolin composite as effective adsorbent for methylene blue removal. *Compos B Engrg* **161**, 141-149. https://doi.org/10.1016/j.compositesb.2018.10.063

Jawad, A.H. and Abdulhameed, A.S. (2020). Facile synthesis of crosslinked chitosan-tripolyphosphate/kaolin clay composite for decolourization and COD reduction of remazol brilliant blue R dye: Optimization by using response surface methodology. Colloids Surf. A: *Physicochem Engrg Asp* **605**, 125329. https://doi.org/10.1016/j.colsurfa.2020.125329

Kimambo, V., Philip, N.Y.J. and Lugwisha, E.H.J. (2014). Suitability of Tanzanian kaolin, quartz and feldspar as raw materials for the production of porcelain tiles. *Int. J. Sci. Technol. Soc.* **2**, 201-209. https://doi.org/10.11648/j.ijsts.20140206.17

Kumar, S., Panda, A.K. and Singh, R. (2013). Preparation and characterization of acid and alkaline treated kaolin clay. Bull. *Chem. React. Engrg. Catal*., **8**, 61-69. https://doi.org/10.9767/bcrec.8.1.4530.61-69

Li, H., Wang, H., Liu, Q., Tan, Y., Jiang, N. and Lin, Y. (2016). Evaporation process for treating high-salinity industrial wastewater at low temperatures and ambient pressure. Desalination and Water Treatment **57**(56): 27048-27060. http://dx.doi.org/10.1080/19443994.2016.1167126

Liu, L., Luo, X., Ding, L. and Luo, S. (2019). Application of nanotechnology in the removal of heavy metal from water In: Luo X, Deng F (eds) Micro and nano technologies, nanomaterials for the removal of pollutants and resource reutilization. *Elsevier*. pp 83-147, ISBN 9780128148372. https://doi.org/10.1016/B978-0-12-814837-2.00004-4

Lugwisha, E.H.J. and Lunyungu, G. (2016). Water defluoridation capacity of Tanzanian kaolin-feldspar blend adsorbents. *American J. Appl. Chem.*, **4**, 77-83. https://doi.org/10.11648/J.AJAC.20160403.12

Lugwisha, E.H.J. and Siafu, S.I. (2014). The properties of feldspathic dental porcelain from Tanzanian aluminosilicate materials. *Int. J. Dev. Res.*, **4**, 2260-2265. http://dspace.nm-aist.ac.tz/handle/123456789/197

Luo, J., Jiang, T., Li, G., Peng, Z., Rao, M. and Zhang, Y. (2017). Porous Materials from Thermally Activated Kaolinite: Preparation, Characterization and Application. *Materials*., **10**(6), 647. https://doi.org/10.3390/ma10060647

Malima, N.M., Owonubi, S.J., Lugwisha, E.H.J. and Mwakaboko, A.S. (2021). Development of cost-effective and eco-friendly adsorbent by direct physical activation of Tanzanian Malangali kaolinite for efficient removal of heavy metals. *Mater Today: Proc* **38**(2), 1126-1132. https://doi.org/10.1016/j.matpr.2020.06.469

Monash, P., Niwas, R. and Pugazhenthi, G. (2011). Utilization of ball clay adsorbents for the removal of crystal violet dye from aqueous solution. *Clean Technol Environ Policy* **13**, 141-151 https://doi.org/10.1007/s10098-010-0292-6

Mudzielwana, R., Gitaria, M.W. and Ndungu, P. (2019). Performance evaluation of surfactant modified kaolin clay in As(III) and As(V) adsorption from groundwater: adsorption kinetics, isotherms and thermodynamics. *Heliyon* **5**, e2756. https://doi.org/10.1016/j.heliyon.2019.e02756

Mulushewa, Z., Dinbore, W.T. and Ayele, Y. (2021). Removal of methylene blue from textile waste water using kaolin and zeolite-x synthesized from Ethiopian kaolin. *Environ. Anal. Health Toxicol*., **36**(1), e2021007. https://doi.org/10.5620/eaht.2021007

.